

TiRE-GAN: Task-Incentivized Generative Learning Models for Radiomap Estimation with Radio Propagation Model

Yueling Zhou*, Achintha Wijesinghe[†], Songyang Zhang*, and Zhi Ding[†], *Fellow, IEEE*

*Department of Electrical and Computer Engineering, University of Louisiana at Lafayette, Lafayette, LA, USA, 70504

[†]Department of Electrical and Computer Engineering, University of California at Davis, Davis, CA, USA, 95616

E-mail: {yueling.zhou1, songyang.zhang}@louisiana.edu, {achwijesinghe, zding}@ucdavis.edu

Abstract—Enriching geometric information on radio frequency (RF) signal power distribution in wireless communication systems, the radiomap has become an essential tool for resource allocation and network management. Usually, a dense radiomap is reconstructed from sparse observations collected by deployed sensors or mobile devices, which makes the radiomap estimation an urgent challenge. To leverage both physical principles of radio propagation models and data statistics from sparse observations, this work introduces a novel task-incentivized generative learning model, namely TiRE-GAN, for radiomap estimation. Specifically, we first introduce a radio depth map as input to capture the overall pattern of radio propagation and shadowing effects, following which a task-driven incentive network is proposed to provide feedback for radiomap compensation depending on downstream tasks. Our experimental results demonstrate the power of the radio depth map to capture radio propagation information, together with the efficiency of the proposed TiRE-GAN for radiomap estimation.

Index Terms—radiomap estimation, generative adversarial networks, radio propagation model

I. INTRODUCTION

The expansion of sensor networks and edge computing systems has stimulated many new technologies in the next generation of wireless communications, such as vehicle-to-everything (v2x) communications [1], unmanned aerial vehicle (UAV)-assisted networking [2] and fifth-generation (5G) terrestrial and non-terrestrial network (NTN) services [3]. All these applications require an accurate description of radio frequency (RF) spectrum coverage and efficient assessment of the radio environment, which lead to the new concept of radiomaps [4]. Describing the RF power spectral density (PSD) over different geometric locations, frequencies, and time, radiomaps can enrich the information of spectrum coverage and assist the aforementioned spectrum management applications [5]. Usually, dense radiomaps are reconstructed from sparse observations collected by mobile sensors and user devices, as shown in Fig. 1. To fully leverage the power of radiomaps in spectrum resource allocation and network optimization, efficient radiomap estimation (RME) from sparse observations has emerged as an urgent challenge.

Existing methods of radiomap estimation can be categorized into model-based or learning-based approaches, each bearing its distinct constraints. Model-based methods usually assume

a specific radio propagation model, with which unknown parameters are estimated by minimizing the error between observed samples and predictions. Typical examples include the log-distance path loss (LDPL) models [6], inverse distance weighted interpolation [7] and thin-plate splines kernels [8]. However, the performances of model-based RME highly rely on the selection of physical radio propagation models, which are usually unknown in practical applications. Moreover, the PSD distribution sometimes is more sensitive to surrounding obstacles rather than following a strict empirical model, especially in complicated environments. The efficient extraction of radio model information from realistic data samples remains an open question.

With the development of artificial intelligence (AI), recent interests of RME focus on learning-based methods [9]. In [10], a fast radiomap estimation is proposed based on Unet. Another work utilizing deep convolutional neural networks is [11], where an auto-encoder structure is presented for radiomap estimation. Other learning-based methods also include the conditional generative adversarial nets (cGAN) [3] and transformers [12]. Despite many successes, efficient learning-based RME requires sufficient data samples with satisfying quality, which are usually inaccessible in realistic scenarios. Although some works [13], [14] consider integrating the radio propagation models with learning machines to address the data scarcity, the efficient model selection remains challenging. Moreover, how to satisfy the special requirements of downstream tasks, such as outage detection and network planning, is another critical concern.

To address the aforementioned problems, this work proposed a **Task-incentivized Radiomap Estimation** based on **Generative Adversarial Networks** (TiRE-GAN) for radiomap estimation, leveraging the synergies of radio propagation model and generative AI. Specifically, a radio depth map is introduced as an additional input channel of the generator to capture the overall radio propagation information and shadowing effects. Then, a task-incentivized block is proposed to provide feedback for radiomap generation to compensate for the estimated PSD based on downstream tasks. Our contributions can be summarized as follows:

- We introduce a novel radio depth map (RDM) as input conditions to the cGAN, serving as a proxy for the shad-

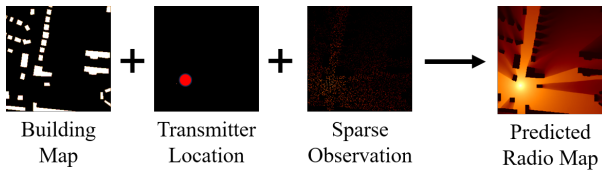


Fig. 1. Problem Description of RME: Given the distribution of buildings, transmitter locations (in red), and the sparse observations collected by mobile sensors and devices, we aim to predict the dense radiomaps.

owing effects and radio propagation behavior, thereby infusing the learning process with additional insights into the physical principles of radio propagation.

- We integrate the physics-conditioned cGAN with a novel task-incentivized network to provide compensation to the estimated radiomaps depending on downstream tasks, which significantly enhances the RME performance.
- Our experimental results demonstrate the power of the proposed radio depth map in characterizing radio propagation behavior, as well as the efficiency of the proposed TiRE-GAN in radiomap estimation.

II. PROBLEM DESCRIPTION

In this section, we first introduce our problem formulation. As shown in Fig. 1, the radiomap estimation is formulated as a sparse sensing problem, where a dense radiomap \hat{M}_R is reconstructed given the landscape information of the surrounding environment, sparse observations collected from sensors and mobile devices, and locations of transmitters, formulated by the following equation:

$$\hat{M}_R = g(M_U, M_T, M_S, \mathcal{X}), \quad (1)$$

where M_U , M_T , M_S and \mathcal{X} represent the landscape map, the encoded transmitter location, the sampled radiomap, and additional extracted features, respectively.

Different from the interpolation formulation in [6] and [7], where the unobserved PSD values are estimated only using the observed samples in the same radiomap, we follow the classic prediction formulation and assume a set of training pairs of (M_R, \mathcal{F}) with $\mathcal{F} = \{M_U, M_T, M_S, \mathcal{X}\}$ to train the mapping function $g(\cdot)$ by

$$\min_{g(\cdot)} L(M_R, \hat{M}_R), \quad (2)$$

where $L(\cdot)$ refers to the designed loss function.

In this work, our objectives can be summarized as two parts: 1) design an effective mapping function $g(\cdot)$ by integrating the cGAN with a novel task-incentivized network; and 2) design a suitable loss function $L(\cdot)$ to embed the physical principles of radio propagation. We shall introduce the details of our proposed TiRE-GAN in Section III.

III. METHODS

A. Overall Structure of TiRE-GAN Framework

We now introduce the overall structure of our proposed TiRE-GAN. As shown in Fig. 2, the architecture of the proposed framework can be structured into three components:

1) model-based data preprocessing; 2) radiomap generation based on cGAN; and 3) task-incentivized feedback.

The overall operational sequence of the training process is delineated as follows. To embed the radio propagation model, the urban landscape map and the transmitter location data are processed to fabricate a physics-embedded Radio Depth Map (RDM), which will be further discussed in Section III-B2. Subsequently, this RDM, alongside the sampled radiomap, urban map, and transmitter location data, are amalgamated into a quadruple-channel input for the cGAN. Throughout the training phase, a pre-trained task-incentivized network is incorporated as a contributory factor within the loss function for the cGAN's generator, enhancing the model's ability to compensate for the radiomap estimations by embedding physics-based constraints and the rewards from downstream tasks. We will then introduce each module as follows.

B. Model-Based Data Preprocessing

The data preprocessing module consists of two parts: 1) process the observed features $\{M_U, M_T, M_S\}$ into aligned inputs of cGAN; and 2) generate a radio depth map embedding the radio propagation behavior.

1) *Observed Data Preprocessing*: Suppose that the radiomap is formatted in a $N \times N$ grid, i.e., $M_R \in \mathbb{R}^{N \times N}$. The landscape map of buildings is encoded as a binary segmented image $M_U \in \mathbb{R}^{N \times N}$, where building areas are marked by 1 and open areas are annotated by 0. Similar to the building map, we encode the transmitter locations into a binary image $M_T \in \mathbb{R}^{N \times N}$, where the transmitter locations are marked as 1; otherwise, the pixel values are zero. The sparse observations can be viewed as the corresponding pixels in gray-scale images $M_S \in \mathbb{R}^{N \times N}$. For convenience, we first use a threshold to eliminate the extremely low-value observations, and then normalize the PSD value into $0 \sim 1$ for the observed locations. Since linear normalization is applied, we can easily re-scale the estimated radiomap back to the original data domain. For the missing values in M_S , we set them as zeros. Since a convolutional neural network is applied for the cGAN structure, zero-padding does not impact the final radiomap estimation.

2) *Radio Depth Map*: To embed the radio propagation information, we introduce the Radio Depth Map (RDM), $\mathcal{X} = M_D \in \mathbb{R}^{N \times N}$ as a novel model-based attribute, derived from the distribution of buildings and the spatial locations of transmitters. Similar to a depth map in computer vision which provides information on the distances of surfaces from a specific viewpoint, the RDM is formulated as:

$$M_D(x, y) = n \left(\sum_{t=1}^{N_T} P_t(x, y) \cdot B_t(x, y) \right), \quad (3)$$

where (x, y) denotes the two-dimensional coordinates of the target location, $P_t(x, y)$ denotes the distance-based path loss gain from the t -th transmitter, and the $B_t(x, y)$ capture the impact of buildings from the viewpoint of t -th transmitter.

Suppose that $C(l, l_t)$ identifies the set of pixels in the direct line of sight between the target location $l = (x, y)$ and location

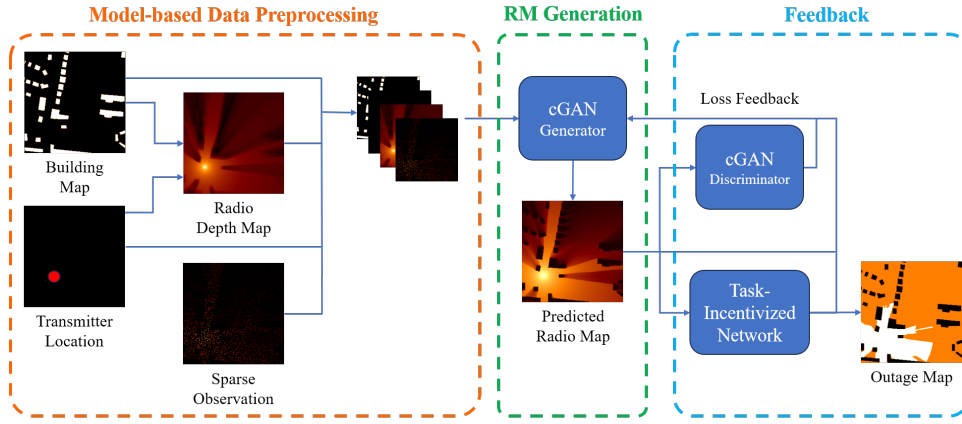


Fig. 2. Overall Structure of TiRE-GAN consisting of 3 parts: 1) The model-based data preprocessing module utilizes the input observed information (e.i. building map and transmitter location) to generate the radio depth map and then stacks the four layers together as input; 2) The radiomap (RM) generation module is in a cGAN generator structure, which learn and produce the prediction of radiomap; 3) The feedback module consists of 2 parts: a cGAN discriminator and a task-incentivized network. Both modules produce a loss term as feedback to improve the generator.

$l_t = (x_t, y_t)$ of the t -th transmitter. The shadowing term impacted by buildings is calculated by

$$B_t(x, y) = \frac{\sum_{i \in C(l, l_t)} (1 - M_U(i))}{\sum_{i \in C(l, l_t)} 1}, \quad (4)$$

which characterizes the ratio of non-building pixels between l and l_t . $B_t(x, y)$ is larger and the shadowing effect is smaller if the radio propagates through fewer buildings.

To capture the path loss $P_t(x, y)$, we employ the Inverse Distance Weighting (IDW) model, calculated by

$$P_t(x, y) = d(l, l_t)^{-\lambda}, \quad \lambda > 0, \quad (5)$$

where $d(l, l_t)$ denotes the Euclidean distance between the target point l and the t -th transmitter. The parameter λ governs the rate, at which signal strength diminishes with increasing distance, necessitating a positive value to ensure physical plausibility in the depth map. An exemplary radio depth map is shown in the orange block of Fig. 2.

C. cGAN Network

In this work, we employ a conditional Generative Adversarial Network (cGAN) [15] as the foundational architecture, which consists of two principal components: a generator G and a discriminator D . Different from the traditional GAN which generates data from random noise, the generator in cGAN can generate data from given features \mathcal{F} and incorporate additional information \mathbf{I} in the discriminator. In our radiomap estimation, the conditional features consist of four channels as processed in the Data Preprocessing Module, i.e., $\mathcal{F} = \{M_U, M_T, M_S, M_D\}$ as shown in Fig. 2. The additional information \mathbf{I} can be designed as a function of the region features, i.e., $\mathbf{I} = h(\mathcal{F})$ or some determined labels, such as fake or real [16]. Then, the basic cGAN can be formulated as

$$\min_G \max_D V(D, G) = \mathbb{E}_{y, \mathbf{I} \sim p_{\text{data}}(\mathbf{y}, \mathbf{I})} [\log D(\mathbf{y}, \mathbf{I})] + \mathbb{E}_{f \sim p_{\text{data}}(\mathcal{F})} [\log(1 - D(G(\mathcal{F}), \mathbf{I}))], \quad (6)$$

where $p_{\text{data}}(\mathbf{y}, \mathbf{I})$ is the joint distribution with the prior knowledge \mathbf{I} , and \mathbf{y} is the generated data. Generally, the

optimization of a min-max problem in cGAN can be split into two sub-problems, and train D and G iteratively. Specifically, the loss function to optimize D is

$$L_D = -V(D, G), \quad (7)$$

and the general loss function to optimize G is

$$L_G = \mathbb{E}_{x \sim p_{\text{data}}(\mathcal{F})} [\log(1 - D(G(\mathcal{F}), \mathbf{I}))]. \quad (8)$$

To leverage both radio propagation model information and data statistics from observed samples, in this work, we will customize the loss function of the generator as

$$L = L_G + \alpha L_{MSE} + \beta L_R. \quad (9)$$

Here, L_{MSE} describes the error of RME by Mean Squared Error (MSE), i.e.,

$$L_{MSE}(\mathbf{y}, \hat{\mathbf{y}}) = \frac{1}{K} \sum_{i=1}^K (y_i - \hat{y}_i)^2, \quad (10)$$

where K is the total number of pixels, \mathbf{y} and $\hat{\mathbf{y}}$ are the ground truth and the predicted radiomap, while y_i and \hat{y}_i are the true and predicted pixel value of the i th pixel. L_R is a task-incentivized regularization term from the feedback module, which will be introduced in Section III-D.

D. Feedback Design

The feedback module consists of two components: 1) a traditional cGAN discriminator; and 2) a task-incentivized network (TIN) based on downstream tasks.

1) *cGAN Discriminator*: Conversely to the cGAN generator, the discriminator aims to detect whether the generated data is fake or not. Here, we consider three-channels as the input of the discriminator, where two are expanded image-sized one-hot encodings representing the binary truthfulness of the input, and the third channel is the generated radiomap. The discriminator outputs a scalar value, indicating the likelihood of whether the provided radiomap is genuine. The

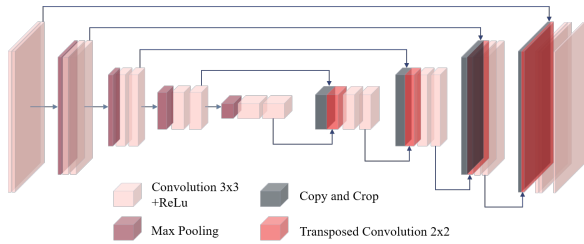


Fig. 3. Task-incentivized network (TIN) structure: We design the TIN based on Unet, which contains 4 encoding blocks and 4 decoding blocks. Each encoding block consists of 3 convolution layers and a pooling layer. Each decoding block consists of one concatenation layer, a transpose convolution layer, and 3 convolution layers.

discriminator is trained by the binary cross entropy (BCE) loss as

$$L_D(\mathbf{y}, \hat{\mathbf{y}}) = -\frac{1}{K} \sum_{i=1}^K [y_i \log(\hat{y}_i) + (1 - y_i) \log(1 - \hat{y}_i)]. \quad (11)$$

2) *Task-Incentivized Network*: In traditional RME, the objective transcends the mere accuracy of radio signal strength at discrete locations within a dense radiomap. However, in practical scenarios, the final objective of RME is to assist spectrum planning and network management. For example, one can easily identify the outage of regions based on their radiomap by setting a certain threshold of service failure. To compensate for the radiomap estimations based on downstream tasks, we introduce a TIN module as shown in Fig. 2.

As an exemplary TIN, we adopt outage detection as a downstream task. More specifically, the proposed TIN utilizes a UNet architecture for semantic segmentation of radio power outage as Fig. 3, where the input constitutes a radiomap and the output is an outage map indicating signal coverage or absence. The training of the TIN is conducted using ground-truth radio coverage and outage maps, thereby ensuring that the network learns to accurately predict outage areas based on real-world data. Once trained, the TIN operates within the cGAN framework as a pre-trained component. During inference, the output generated by the cGAN’s generator serves as the input to the TIN, enabling it to contribute an additional term L_R to the loss function of the cGAN. This term is specifically designed to encapsulate aspects of human-centric interest, such as the distribution and characteristics of signal outages, thereby guiding the cGAN toward generating radiomaps that are not only precise but also aligned with the real-world considerations and requirements of downstream tasks. This integration of the TIN within the cGAN architecture exemplifies a strategic convergence of machine learning precision with domain-specific insights, enhancing the utility and applicability of the generated radiomaps.

The TIN provides the task-incentivized regularization term L_R in the loss function of the generator, which is calculated by the pre-trained TIN using the MSE loss to measure the error between the predicted and the ground truth outage maps:

$$L_R(z, \hat{z}) = \frac{1}{K} \sum_{i=1}^K (z_i - \hat{z}_i)^2, \quad (12)$$

where the z and \hat{z} are the ground truth and the predicted outage map, while z_i and \hat{z}_i are the true and predicted pixel values of the i th pixel. K is the number of pixels.

Note that, our TIN can be integrated with any RM-assisted applications. Some other typical examples also include ray tracing or wireless localization.

IV. EXPERIMENTS

A. Experiment Setup

1) *Data description*: In this work, we utilize the RadiomapSeer dataset [10] for evaluation, which comprises an extensive set of 700 maps from a variety of metropolitan areas, including Ankara, Berlin, Glasgow, Ljubljana, London, and Tel Aviv. Each map delineates a quadrant of 256×256 square meters, depicted with a granularity of 256×256 pixels. The edifices are encoded by assigning a pixel intensity of one, whereas open spaces are represented by a zero value. Furthermore, the precise locations of transmitters are encoded with a pixel intensity of one superimposed on a null background, facilitating accurate localization.

2) *Method Comparison*: To evaluate the performance of our TiRE-GAN, we compare with both state-of-the-art (SOTA) model-based methods, including **Kriging** [17], and data-driven approaches, including **Matrix completion (MC)** [18], **AutoEncoder (AE)** [11], **RadioUnet (RU)** [10] and conventional **cGAN** [15]. For the interpolation-based method, we reconstruct the radiomap with observations in the same radiomap. For the prediction-based method, we split the dataset as 4000/800/800 (70%/15%/15%) for training/validation/testing sets. In our TiRE-GAN, we set $\alpha = 1$ and $\beta = 0.1$ in Eq. (9).

B. Overall performance

We first present the overall performance of different radiomap estimations under different sampling ratios (sr). In this work, we evaluate the performance based on the normalized radiomaps via MSE denoted by

$$\text{MSE}(\mathbf{y}, \hat{\mathbf{y}}) = \frac{1}{K} \sum_{i=1}^K (y_i - \hat{y}_i)^2, \quad (13)$$

and normalized MSE (NMSE) calculated by

$$\text{NMSE}(\mathbf{y}, \hat{\mathbf{y}}) = \frac{1}{K} \sum_{i=1}^K \frac{(y_i - \hat{y}_i)^2}{y_i^2}, \quad (14)$$

where $K = 256^2$. Note that, since the linear normalization is applied, we can easily re-scale the estimated radiomap back to the original data domain. The results are presented in Table I and II. From the results, our proposed TiRE-GAN always achieves superior performance against all other SOTA approaches. Specifically, with the assistance of our proposed radio depth map, our method can achieve a very high reconstruction accuracy even with a very small sampling ratio and insufficient training samples, which validates the effectiveness of the proposed method. The visualization results of different methods in 3 radiomap examples are shown in

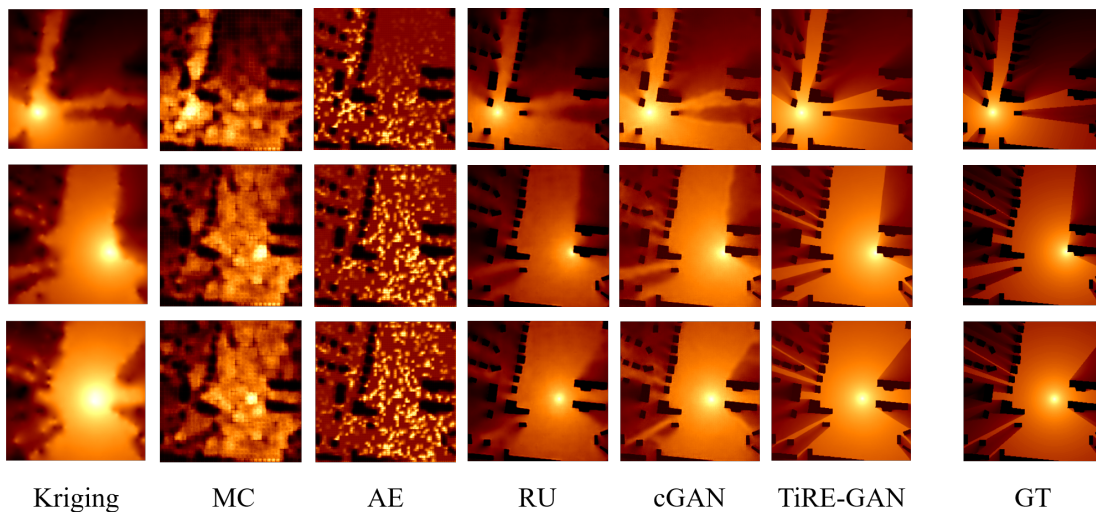


Fig. 4. Performance comparison (sr=1) between Kriging, matrix completion(MC), AutoEncoder (AE), RadioUNet (RU), conditional GAN (cGAN), our TiRE-GAN, and the ground truth (GT) on 3 radiomap examples. TiRE-GAN achieves the best radio propagation and the shadowing effect prediction.

TABLE I
TEST NMSE COMPARISON ($\times 10^{-2}$)

sr (%)	0.03	0.1	0.5	1	3	5	10	Average
Krigin	24.5696	18.9280	14.2451	12.9608	14.7171	11.3540	10.9647	15.3913
RU	6.5421	5.1111	2.6374	2.2206	1.8192	1.5191	1.2704	2.8744
AE	54.7656	53.8440	45.6640	43.3302	26.0041	20.7167	14.3275	36.9503
AE deep	50.6597	48.8197	21.4272	16.2537	6.8252	6.5503	5.8179	156.3537
cGAN	11.5754	5.4805	2.1345	1.8301	1.3009	1.1894	1.0295	3.5057
MC	83.0969	74.7810	69.0133	66.9996	62.8215	56.3645	55.4314	66.9297
TiRE-GAN	1.9866	1.2608	0.7282	0.6084	0.5228	0.5119	0.4615	0.8686

TABLE II
TEST MSE COMPARISON ($\times 10^{-4}$)

sr (%)	0.03	0.1	0.5	1	3	5	10	Average
Krigin	188.7554	141.3767	110.7954	101.5476	91.9940	89.0443	86.0208	115.5340
RU	24.6458	19.3893	10.0221	8.4693	7.0856	5.9640	4.9978	11.5105
AE	230.6564	226.6141	194.4702	186.5724	113.0439	87.7205	65.0134	157.7272
AE deep	209.2621	201.4013	91.9589	70.0012	26.8177	26.4321	23.4719	92.7636
cGAN	45.8797	22.0908	8.4572	7.2467	5.0700	4.6442	4.0541	13.9203
MC	342.1892	307.9448	284.1937	275.9010	258.6960	232.1065	228.2640	275.6136
TiRE-GAN	7.0604	4.6453	2.7678	2.3472	2.0377	2.0015	1.8137	3.2390

Fig. 4, where the sample ratio is 1%. From the visualization results, the radioUnet, cGAN, and TiRE-GAN have better performances than Kriging, MC, and AE in capturing the overall radio propagation patterns. Compared to radioUnet and cGAN, our TiRE-GAN has more explicit boundaries for the shadowing effects, resulting from the compensation from the TIN feedback. The numerical results, together with the visualization results demonstrate the efficiency of our proposed TiRE-GAN for radiomap estimation.

C. Robustness Against Noise

To evaluate the robustness of TiRE-GAN, we conduct the experiment, where a noisy input pattern is substituted for the original sparse observation channel by introducing additive Gaussian noise to each sampled value in the radiomap. To showcase the effectiveness of the proposed radio depth map and TIN blocks, we compare our TiRE-GAN with Kriging, matrix completion(MC), AutoEncoder (AE), RadioUNet

(RU), and conditional GAN (cGAN) under different signal-to-noise ratios (SNR) as Fig. 5. Here, we consider a sampling ratio of 1% for all the test cases. From the results, our TiRE-GAN always has better performance. Moreover, the MSE of TiRE-GAN increases slower than those of other methods, especially compared to the high performance methods (RadioUNet, cGAN), demonstrating the robustness of the TiRE-GAN against noise.

D. Outage Evaluation of Generated radiomap

To further evaluate the performance of reconstructed radiomaps in downstream tasks, we compare the performance of RM-assisted outage detection. Here, we input the generated radiomaps from different methods into the pre-trained outage detection networks. The numerical results of the whole datasets with sr=1% and the exemplary visualization results are shown in Table III and Fig. 6, respectively. From the results, the traditional model-based methods and conventional

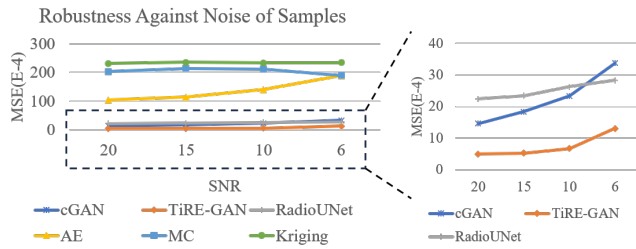


Fig. 5. The MSE ($\times 10^{-4}$) of Kriging, matrix completion(MC), AutoEncoder (AE), RadioUNet (RU), conditional GAN (cGAN), and TiRE-GAN of different SNRs under a sample ratio=1%.

TABLE III
OUTAGE MAP MSE COMPARISON

Method	Kriging	MC	AE
MSE	0.078134	0.075765	0.049377
Method	RU	cGAN	TiRE-GAN
MSE	0.028439	0.030352	0.026682

auto-encoder perform poorly in the outage detection. Our TiRE-GAN always has superior performance, which demonstrates the effectiveness of TIN in radiomap compensation for downstream tasks.

V. CONCLUSION

In this work, we introduce a task-incentivized generative learning model, namely TiRE-GAN for radiomap estimation. More specifically, to characterize the overall radio propagation behavior, we introduce a radio depth map as additional physics-embedded features as the condition to guide the data-driven generative models. To compensate for the radiomap estimation for downstream tasks, we introduce a task-incentivized network to provide feedback to predict the detailed features in the radiomap. From our experimental results, the proposed TiRE-GAN always achieves superior performance, even with insufficient training samples, which addresses the barriers of conventional learning approaches. Our numerical and visualization results demonstrate the effectiveness of the proposed radio depth map and TiRE-GAN. Future research endeavors will delve into the optimization of the generator’s reward mechanism. Another promising direction is the multi-band radiomap estimation for different frequencies.

REFERENCES

- [1] S. Roger, M. Brambilla, B. C. Tedeschini, C. Botella-Mascarell, M. Cobos and M. Nicoli, “Deep-learning-based radiomap reconstruction for v2x communications,” in *IEEE Transactions on Vehicular Technology*, vol. 73, no. 3, pp. 3863-3871, Mar. 2024.
- [2] N. Zhao, W. Lu, M. Sheng, Y. Chen, J. Tang, F. R. Yu, and K. Wong, “Uav-assisted emergency networks in disasters,” in *IEEE Wireless Communications*, vol. 26, no. 1, pp. 45-51, Feb. 2019.
- [3] S. Zhang, A. Wijesinghe and Z. Ding, “RME-GAN: a learning framework for radiomap estimation based on conditional generative adversarial network,” in *IEEE Internet of Things Journal*, vol. 10, no. 20, pp. 18016-18027, Oct. 2023.
- [4] S. Bi, J. Lyu, Z. Ding and R. Zhang, “Engineering radiomaps for wireless resource management,” in *IEEE Wireless Communications*, vol. 26, no. 2, pp. 133-141, Apr. 2019.

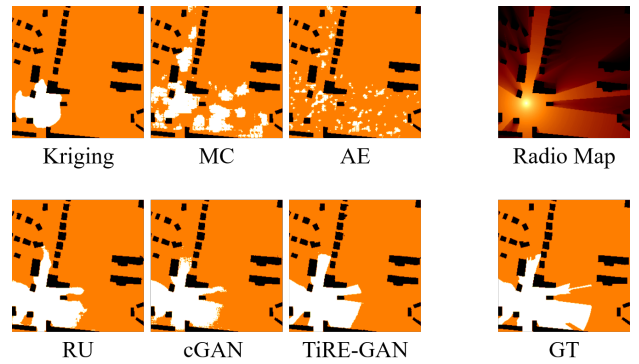


Fig. 6. Illustration of Outage Map Prediction under $sr=1\%$. We compared the outage map predicted by the generated radiomap from Kriging, matrix completion(MC), AutoEncoder (AE), RadioUNet (RU), conditional GAN (cGAN), and our TiRE-GAN. The corresponding radiomap and the ground truth outage map(GT) are shown on the right for reference. The result shows that TiRE-GAN has the best capability to predict the outage map with a clear boundary and range.

- [5] S. Debroy, S. Bhattacharjee and M. Chatterjee, “Spectrum map and its application in resource management in cognitive radio networks,” in *IEEE Transactions on Cognitive Communications and Networking*, vol. 1, no. 4, pp. 406-419, Dec. 2015.
- [6] M. Lee and D. Han, “Voronoi tessellation based interpolation method for wi-fi radiomap construction,” in *IEEE Communications Letters*, vol. 16, no. 3, pp. 404-407, Mar. 2012.
- [7] S. -P. Kuo and Y. -C. Tseng, “Discriminant minimization search for large-scale rf-based localization systems,” in *IEEE Transactions on Mobile Computing*, vol. 10, no. 2, pp. 291-304, Feb. 2011.
- [8] J. A. Bazerque, G. Mateos, and G. B. Giannakis, “Group-Lasso on splines for spectrum cartography,” in *IEEE Trans. Signal Process.*, vol. 59, no. 10, pp. 4648-4663, Oct. 2011.
- [9] D. Romero and S. -J. Kim, “radiomap Estimation: A data-driven approach to spectrum cartography,” in *IEEE Signal Processing Magazine*, vol. 39, no. 6, pp. 53-72, Nov. 2022.
- [10] R. Levie, Ç. Yapar, G. Kutyniok and G. Caire, “Radiounet: fast radiomap estimation with convolutional neural networks,” in *IEEE Transactions on Wireless Communications*, vol. 20, no. 6, pp. 4001-4015, Jun. 2021.
- [11] Y. Teganya and D. Romero, “Deep completion autoencoders for radiomap estimation,” in *IEEE Trans. Wireless Commun.*, vol. 21, no. 3, pp. 1710-1724, Mar. 2022.
- [12] Y. Tian, S. Yuan, W. Chen and N. Liu, “Transformer based radiomap prediction model for dense urban environments,” in *Proc. 13th International Symposium on Antennas, Propagation and EM Theory (ISAPE)*, Zhuhai, China, 2021, pp. 1-3.
- [13] S. Zhang, T. Yu, B. Choi, F. Ouyang and Z. Ding, “Radiomap inpainting for restricted areas based on propagation priority and depth map,” in *IEEE Transactions on Wireless Communications*, Feb. 2024.
- [14] Y. Zheng, J. Wang, X. Li, J. Li and S. Liu, “Cell-level rsrp estimation with the image-to-image wireless propagation model based on measured data,” in *IEEE Transactions on Cognitive Communications and Networking*, vol. 9, no. 6, pp. 1412-1423, Dec. 2023.
- [15] M. Mirza and S. Osindero, “Conditional Generative Adversarial Nets,” arXiv:1411.1784, Nov. 06, 2014.
- [16] Y. Liu, Z. Qin, T. Wan, and Z. Luo, “Auto-painter: cartoon image generation from sketch by using conditional wasserstein generative adversarial networks,” in *Neurocomputing*, vol. 311, pp. 78-87, Oct. 2018.
- [17] K. Sato and T. Fujii, “Kriging-based interference power constraint: integrated design of the radio environment map and transmission power,” in *IEEE Transactions on Cognitive Communications and Networking*, vol. 3, no. 1, pp. 13-25, Mar. 2017.
- [18] Z. Wang, L. Zhang, Q. Kong, and K. Wang, “Fast construction of the radiomap based on the improved low-rank matrix completion and recovery method for an indoor positioning system,” *Journal of Sensors*, pp. 1-12, Oct. 2021.